Journal of Applied Electrochemistry (2006) 36:507–522
DOI 10.1007/s10800-006-9120-4

Reviews in Applied Electrochemistry Number 60

Progress in the synthesis of carbon nanotube- and nanofiber-supported Pt electrocatalysts for PEM fuel cell catalysis

KUNCHAN LEE[1], JIUJUN ZHANG[1,*], HAIJIANG WANG[1] and DAVID P. WILKINSON[1,2]
[1]*Institute for Fuel Cell Innovation, National Research Council Canada, Vancouver, BC, Canada, V6T 1W5*
[2]*Department of Chemical and Biological Engineering, University of British Columbia, Vancouver, BC, Canada, V6T 1Z4*
*(*author for correspondence, fax: + 1-604-221-3001, e-mail: jiujun.zhang@nrc.gc.ca)*

Received 22 August 2005; accepted in revised form 6 January 2006

Key words: carbon nanofiber, carbon nanotube, catalyst supports, electrocatalyst, oxygen electroreduction, PEM fuel cells, synthesis

Abstract

This paper reviews the literature on the synthesis of carbon nanotube- and nanofiber-supported Pt electrocatalysts for proton exchange membrane (PEM) fuel cell catalyst loading reduction through the improvement of catalyst utilization and activity, especially focusing on cathode nano-electrocatalyst preparation methods. The features of each synthetic method were also discussed based on the morphology of the synthesized catalysts. It is clear that synthesis methods play an important role in catalyst morphology, Pt utilization and catalytic activity. Though some remarkable progress has been made in nanotube- and nanofiber-supported Pt catalyst preparation techniques, the real breakthroughs have not yet been made in terms of cost-effectiveness, catalytic activity, durability and chemical/electrochemical stability. In order to make such electrocatalysts commercially feasible, cost-effective and innovative, catalyst synthesis methods are needed for Pt loading reduction and performance optimization.

1. Introduction

Proton exchange membrane (PEM) fuel cells have drawn a great deal of attention in both fundamental and application in recent years [1]. As the energy converting devices used in transportation, stationary, portable and micropower, PEM fuel cells have unique and favourable advantages over chemical batteries in terms of high efficiency, high energy density, and zero or low emission. From the 1960s to the present, great progress has been made in the research and development of PEM fuel cells in terms of stack power density increases and cost reduction [1].

With regard to PEM fuel cell stack power improvement [2], the power density has significantly increased from $\sim$0.1 kW l^{-1} in 1989 to 2.3 kW l^{-1} in 2001. With further development, the power density is expected to exceed 3000 kW l^{-1} in 2010 [2]. For stack component cost reduction, platinum catalyst loading has been reduced by a factor of more than 100. However, these improvements are still not enough according to the US Department of Energy (DOE) reports [3]. The cost of the current PEM fuel cell stack is estimated to have dropped from \$275 kW^{-1} in 2002 to \$175 kW^{-1} in 2004 [3]. The targets of the DOE are to achieve less than \$45 kW^{-1} by 2010 and \$30 kW^{-1} by 2015 in order to be competitive with gasoline-hybrid engine technologies [3].

In order to reach the DOE cost reduction targets, among other component cost reductions, the total Pt catalyst loading in a membrane electrode assembly (MEA) must be reduced to $\sim$0.03 mg cm^{-2} [3]. For Pt catalyst reduction, two approaches are currently very active: exploration of non-noble catalysts, and reduction of Pt loading [4]. With respect to non-noble catalysts, there have been no significant breakthroughs in the areas of materials and technology. Although some promising approaches and results have been reported for Pt loading reduction through alloying, nano-particle supporting tactics, etc., the lifetime of a low Pt loading fuel cell is still problematic.

In this review paper we are focusing on the approach of carbon nanotube- and nanofiber-supported Pt catalysts and their synthesis methodological development. As discussed above, under the strong driving force of fuel cell cost reduction and performance optimization towards commercialization, carbon nanotubes (CNTs) and nanofibers (CNFs), as the novel catalyst supports for increasing Pt utilization, have, since the 1990s, drawn a great deal of attention due to their unique surface structure, high electric conductivity and large

surface areas. The main purposes for using CNT- and CNF-supported Pt catalysts are to reduce Pt loading through increasing the catalyst utilization, and improving the catalyst activity/performance.

It is generally recognized that one of the big advantages of the PEM fuel cell stack is its fitness in the automobile industry as the zero-emission power supply. The number of automobiles in the world is expected to exceed 1.5 billion in 2020 [5]. At the current level of the state-of-the-art technology (cathode Pt loading: 0.4 mg cm^{-2}, and anode: 0.05 mg cm^{-2}), the Pt storage in the earth would be short if each car that is powered by a 100 kW fuel cell stack needs 100 g Pt [6, 7]. One and one half billion cars would need 150 000 tons of Pt. However, the total Pt resources in the world are estimated to be ~28 000 tons [5], which could only supply ~20% of all automobiles. If there are 1.5 billion automobiles, all powered by a fuel cell stack by 2020, the Pt loading must be reduced by a factor of 10.

Another major factor may be the Pt catalyst cost, which could become a barrier towards fuel cell commercialization. Table 1 shows the breakdown of fuel cell stack costs based on the power cost of \$140 kW^{-1} [8]. In this estimation, the noble metal contents in the MEA are Pt/Ru 0.4/0.2 mg cm^{-2} for the anode and Pt 0.4 mg cm^{-2} for the cathode (the total Pt content is 180 g per stack). The total catalyst layer makes up 50% of the stack cost, in which the catalyst cost is about 70%. Therefore, without sharply reducing Pt loading at both the cathode and anode, it is not likely to realize fuel cell commercialization [1, 3, 4, 7–9].

It is very difficult to maintain or improve catalyst layer performance when the catalyst loading is reduced. In order to achieve that, great effort must be put on Pt utilization and the enhancement of catalyst activity. The main focus of this paper will be on cathode oxygen reduction catalysis. The kinetics of cathode oxygen reduction on Pt is relatively slow compared to that of anode hydrogen oxidation. Therefore the large overpotential for the oxygen reduction reaction (ORR) has been a major issue in PEM fuel cell performance [10, 11]. As shown in Figure 1, the overpotential for ORR contributes a major portion (~80%) of the total cell voltage losses [2, 12, 13]. Reducing the overpotential of ORR at the cathode is very critical to improvement of the efficiency of the PEM fuel cell performance. In order to improve the efficiency of the cathode, the following methods have been suggested: (1) increasing catalyst activity towards ORR, (2) increasing the utilization of Pt within the electrode through the high dispersion of the catalyst and (3) improving the catalyst layer structure [6, 14].

Many approaches have been reported for Pt catalytic activity enhancement towards ORRs in fuel cell applications [14–18]. In particular, the Pt-transition metal alloys have attracted much interest due to their enhanced catalytic activities towards ORR in phosphoric acid fuel cell and PEM fuel cell developments. United Technologies Corporation (UTC) reported the first Pt alloying research on ORR catalysis for the phosphoric acid fuel cell in 1980 [15]. Mukerjee et al. [19] reported Pt alloy catalysts for PEM fuel cells in 1993. In these reports, the carbon-supported Pt/Cr, Pt/Co and Pt/Ni alloy catalysts showed a performance gain of 20–30 mV over Pt at low current density range. From 1995 to 1997, Johnson Matthey investigated carbon-supported Pt alloys (Pt/Fe, Pt/Mn, Pt/Ni, Pt/Ti, Pt/Cr and Pt/Cu) for PEM fuel cells [6, 15], demonstrating that Pt/Ti, Pt/Mn and Pt/Fe catalysts could enhance fuel cell performance by 20–40 mV at a practical current density range. Tafel slopes of ca. 60 mV dec^{-1} were found for Pt alloys, which are similar to that of pure Pt catalysts, suggesting that the ORR mechanisms may not be changed significantly. Recently, ternary Pt alloys together with binary Pt alloys have been developed. Tamizhmani et al. reported that a carbon-supported Pt/Cr/Cu ternary alloy showed two times greater activity towards ORR than pure Pt. The mixture of Pt/Cr/Cu alloy with base metal oxides such as copper oxide and chromium oxide could enhance the activity by a factor of 6 compared to

Table 1. Breakdown of fuel cell stack costs (50 kW_e net, 500 000 units per year) [8]

Component	Cost		
	%	\$	\$$kW^{-1}$
MEA			
Cathode and anode layer	50	3625	75
Electroyte	20	1310	25
GDL	5	420	5
Bipolar plates	15	1035	20
Gaskets	5	380	10
Other	5	28	5
Total	100	7050	140

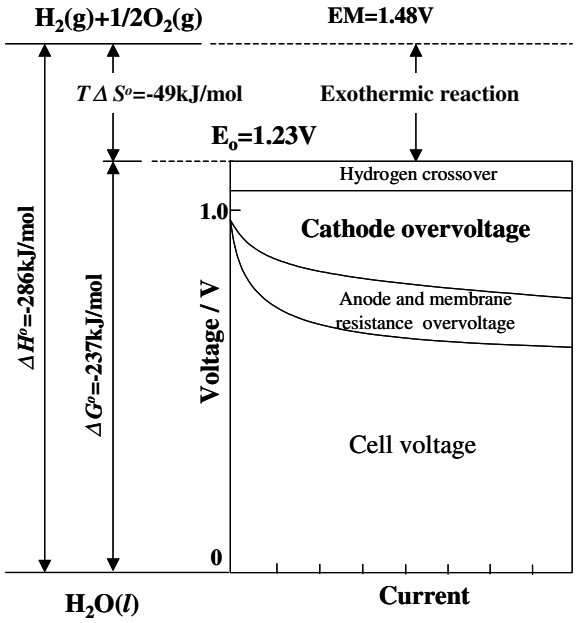

Fig. 1. Overpotential components in PEFCs. Reproduced from [12].

a pure Pt catalyst [20]. More recently, Toda et al. employed a sputtering method and successfully prepared the Pt/Ni, Pt/Co and Pt/Fe alloy catalysts [13]. Although the catalytic activities of these Pt alloys were not validated in a real fuel cell operating condition, the claimed increase in maximum activity could be 10, 15, and 20 times higher than a pure Pt catalyst when the Ni, Co and Fe contents in the Pt alloy catalysts were ca. 30%, 40% and 50%, respectively.

It is obvious that the approach of Pt alloying with non-noble transition metals can create some active alloy catalysts for catalytic activity enhancement towards ORR. However, there are many concerns about the long-term stability of these Pt-alloy catalysts due to the leaching issue of the non-noble metals under the cathode operating environment. The leaching of non-noble metal from the Pt-alloy may cause the following problems: (1) catalytic activity degradation or loss, (2) membrane proton conductivity degradation by metal ionic contamination, and (3) cathode catalyst layer resistance increase [6, 14].

Another attempt for MEA Pt loading reduction has been focusing on improving the utilization of Pt through increasing the reactive surface area [14, 21]. Pt can be supported on some high-surface-area, electronically conductive substrates such as carbon particles to form supported catalysts. Carbon blacks with a high degree of graphitic character, i.e., Vulcan XC-72R, Black Pearls 2000, Ketjen Black, etc., have been commonly used as catalyst supports in the PEM fuel cell MEA preparation [14, 21]. In this way, some uniformly and highly dispersed Pt nanoparticles can be obtained and the reactive surface area of the catalyst can be increased significantly. Carbon-supported Pt catalysts have been suggested to be more favourable than that of non-supported Pt catalysts in catalyst agglomeration prevention under fuel cell operating conditions [21].

In terms of catalyst supporting strategies, the most active area of research is in carbon nanotube (CNT) and nanofiber (CNF) supported Pt catalysts for Pt utilization improvement. Since the discovery of CNF and CNT in 1889 and 1991, respectively, they have attracted great attention throughout the world [22, 23]. A significant amount of work has been done in the past decade to investigate the unique structural, mechanical, electromechanical, and chemical properties of CNT/CNF [24]. In comparison with the most widely used Vulcan XC-72R carbon support which has an electronic conductivity of 4.0 S cm^{-1} and specific surface area of 237 m^2 g^{-1} [25], CNT and CNF have significantly higher electronic conductivities of 10^4 and 10^3–10^4 S cm^{-1}, respectively [26, 27] and extremely high specific surface areas of 200–900 m^2 g^{-1} [27]. Furthermore, Vulcan XC-72R has a large ratio of micropores which are smaller than 2 nm, while CNT and CNF have no micropores smaller than 2 nm [25]. For Vulcan XC-72R support, the Pt nanoparticles may sink into the micropores, which will reduce the number of three-phase boundary reactive sites, thus reducing the Pt utilization [28, 29]. The unique surface structures and excellent mechanical and thermal properties of CNT/CNF, as well as their high electric conductivity and surface area are expected to offer great potential for catalyst supports [27, 30]. However, since CNT and CNF are relatively inert, it is necessary to modify the nature and concentration of surface functional groups in order to deposit Pt particles on their surface [27, 30]. Therefore their pretreatment process and Pt deposition methods could affect the Pt catalyst dispersion and catalytic activity for fuel cell reactions. Various methods have been reported on the synthesis of Pt/CNT and Pt/CNF catalysts. The synthesis methods, which are critical for Pt/CNT and Pt/CNF catalyst preparation, should play a vital role in Pt utilization increase.

Although there have been many reviews dealing with the synthesis of CNT and CNF and their characteristics as a novel catalyst support in catalyst preparation [24, 27, 30–34], there are few published reviews which have emphasized the PEM fuel cell application. Thus, this paper reviews recent works on the synthesis methods of the Pt electrocatalyst using CNTs and CNFs as supports with emphasis on the PEM fuel cell catalysis. The features of reviewed synthesis methods and the electrocatalytic activities of synthesized Pt/CNT and Pt/CNF catalysts for PEM fuel cell reactions will also be discussed based on the morphology of the catalysts.

2. Synthetic methods for Pt/CNT and Pt/CNF electrocatalysts

In PEM fuel cell catalysis, as discussed above, there are essentially two types of nanoparticle-supported Pt catalysts, i.e., carbon nanotube-supported Pt catalysts and nanofiber-supported catalysts. In the following section, the synthetic methods corresponding to each kind of supported catalyst will be reviewed separately.

2.1. *Pt/carbon nanotube (Pt/CNT) catalysts*

From 1991 to the present, the synthesis of carbon nanotubes, a cutting-edge technique, has been developed significantly and some great successes have been made by many scientists in the fields of science and technology, especially in the area of nanotechnology [23, 35]. The most successful synthetic method for CNT preparation is the catalytic decomposition of gas or solid containing carbons.

Figure 2 shows two types of carbon nanotubes, the single-wall carbon nanotube (SWNT) and the multi-wall carbon nanotube (MWNT). The SWNT is a seamless cylinder enclosed by a single graphene sheet. The tube's diameters are normally distributed in a range of 0.4–3 nm and their length is usually in the order of micrometers. The SWNTs usually come together to form some bundles. In a bundle, the SWNTs are hexagonally arranged to form a crystal-like structure [35]. The MWNT can be considered as a concentric

SWNT with an increasing diameter and is coaxially disposed. The number of walls present can vary from two (double wall nanotubes) to several tens, so that the external diameter can reach up to 100 nm. The concentric walls are regularly spaced by 0.34 nm, which is similar to the intergraphene distance in turbostratic graphite materials [27].

For the synthesis of CNTs, the most common techniques are chemical vapour deposition, arc-discharge evaporation, and laser vaporization synthesis [24, 31]. The synthesis conditions (i.e., temperature, pressure, carrier gas, etc.), the types of metal catalyst (i.e., platinum, iron, nickel, cobalt, etc.), and the carbon sources (i.e., graphite, hydrocarbon, etc.) have shown great influence on the properties of the resulting CNTs. For Pt/CNT and Pt/CNF catalyst synthesis, the surface treatment to the CNT surface to create some functional groups for Pt particle deposition is a very important step towards an active fuel cell cathode catalyst. The following methods will address this issue.

2.1.1. *Electroless deposition (conventional impregnation method)*

The electroless deposition method (i.e., the conventional impregnation method) is the most widely used method for highly dispersing Pt nanoparticles on the carbon support in a PEM fuel cell catalyst preparation. Figure 3 shows the typical preparation procedure of the electroless deposition method for Pt/CNT catalysts [25, 36, 37]. It is worthwhile to point out that the as-produced CNT does not possess a high number of surface functional groups on its tube surface. Some defects located on the CNT surface can serve as anchoring sites for catalyst metals [27, 37–43]. Therefore the surface activation step to create surface active sites is essential in order to improve the dispersion of catalyst metals on the CNT surface. The aromatic conjugate ring structure of the CNT surface can be modified by an oxidation process of extremely aggressive reagents (HNO_3 or H_2SO_4 or a mixture of two), resulting in some functional groups on the CNT surface such as hydroxyl (–OH), carboxyl (–COOH) and carbonyl (–C=O) [37–40]. These surface functional groups roughly have a site ratio of 4 (–OH):2 (–COOH):1 (–C=O) [41]. These groups are expected to facilitate the chemical interaction between the anchoring catalyst metal ions and the modified CNT surface. A typical example of chemical interaction between anchoring catalyst metal ions with a CNT functional surface could be proposed as Equation (1) [42]:

$$\mathrm{CNT{-}COOH} + \mathrm{M^+X^-} \rightarrow \mathrm{CNT{-}COO^-M^+} + \mathrm{HX} \quad (1)$$

where the carboxylic group on the CNT surface exchanges a proton with a metal ion (M^+).

Yu et al. proposed a mechanism of Pt deposition on the CNT surface via oxidation of $HNO_3 + H_2SO_4$ [40]. As shown in Figure 4, when CNTs are refluxed with a mixture of $HNO_3 + H_2SO_4$, the CNT graphite surfaces will react with the oxidants and produce a high density of various surface functional groups including carboxyl, carbonyl and phenolic groups. Upon the introduction of Pt^{2+} ions into this system, Pt ions will interact with the surface and attach onto surface functional groups through an ion exchange or coordination reaction. This step is used to create some nucleation precursors. Upon the addition of a reductive agent such as H_2, HCHO or ethylene glycol into the reaction system, the surface Pt^{2+} could be reduced to well-dispersed Pt metal nanoparticles, resulting in a Pt/CNT catalyst. Usually, prior to the surface oxidation treatment, the CNTs must be purified by an ultrasonic treatment or acid treatment in order to remove the contaminants, and then refluxed by 70% HNO_3 at a temperature range of 120–140 °C over 4 h to obtain surfaced-oxidized CNTs [25, 29, 37, 39].

Rajalakshmi et al. investigated the effect of surface oxidation pre-treatment on the Pt decoration [37]. They prepared three types of MWNT with different oxidation treatments: (1) non-oxidized MWNT, (2) sonicated MWNT for wetness, and (3) surface-oxidized MWNTs using 70% nitric acid. Pt particles were deposited on the MWNT surfaces through a chemical reduction of H_2PtCl_6 by $NaBH_4$. Surface-oxidized MWNTs showed smaller Pt nanoparticle size (3–5 nm) and more uniform

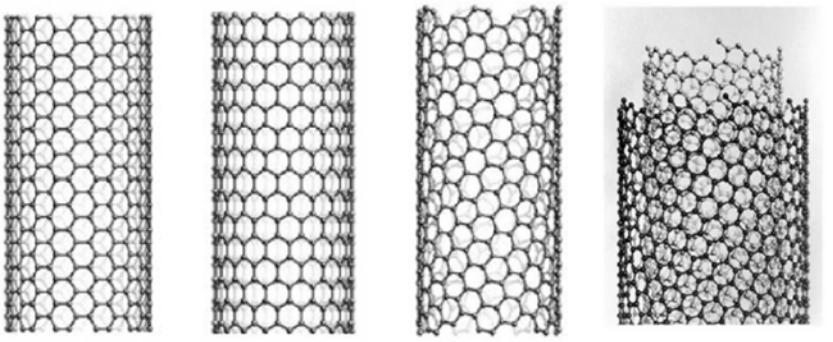

(a) Single-wall CNT **(b)** Multi-wall CNT

Fig. 2. Various types of CNTs [35].

Pt particle distribution compared with those of non-oxidized MWNTs. This result further confirms that the chemical interaction between the functional surface group of oxidized MWNT and the Pt ion can make a molecular level distribution of Pt ions over the MWNT surface and form smaller Pt particle sizes upon reduction of Pt ion. When the oxidized MWNT-supported Pt catalysts were used as the cathode catalyst, a cell voltage of 680 mV at 500 mA cm^{-2} was obtained at fuel cell operating conditions, whereas the other two catalysts gave a lower performance (~40 mV lower). On the other hand, when Pt ions were reduced by ethylene glycol on an oxidized MWNT surface, the formed MWNT-supported Pt catalyst showed larger Pt nanoparticle size (~12–15 nm) and its corresponding fuel cell performance was also lower (~638 mV at 500 mA cm^{-2}) than the case where Pt ions were reduced by $NaBH_4$.

Liu et al. reported that the surface functionalization of MWNTs by a two-step sensitization-activation treatment was more effective for high Pt dispersion and catalytic activity enhancement than conventional surface oxidation treatment [39]. The first step in the two-step sensitization-activation pre-treatment was to oxidize the raw CNTs by either a 70% HNO_3 solution at 140 °C; or a mixture of 98% HNO_3 + 70% H_2SO_4 solution at 140 °C; or a 0.38 M $K_2Cr_2O_7$ + 4.5 M H_2SO_4 solution at 60 °C. In the second step, the oxidized CNTs were ultrasonicated in a sensitizing solution (0.1 M $SnCl_2$ + 0.1 M HCl) for 1 h at room temperature. After filtration, CNTs were activated in 0.0014 M $PdCl_2$ + 0.25 M HCl solution for another 0.5 h by ultrasonic treatment. Finally, the resultant CNTs were decorated in a Pt electroless plating solution for Pt particle deposition to produce a Pt/CNT catalyst. Based on X-ray photoelectron microscopy (XPS), they found that a high density of surface functional groups was produced on the CNT surfaces by HNO_3, or $K_2Cr_2O_7$ + H_2SO_4 oxidation. The yield of functionalized CNTs was about 93% if the oxidation agent was HNO_3, and 91% if the oxidation agent was $K_2Cr_2O_7$ + H_2SO_4. In particular, the Pt/CNT catalyst with $K_2Cr_2O_7$ treatment showed smaller Pt nanoparticle sizes (1–5 nm), although the partial agglomeration of Pt nanoparticles could be observed in a transmission electron microscope (TEM) analysis. They also found that the aging time of the sensitizing solution played an important role in the two-step process [39]. The aging effect was examined in the aging time periods of 1, 3, 6, 9, 12, and 15 days. The optimum aging time was observed to be 3 days for high dispersion of Pt nanoparticles on the sensitized CNT surface.

The fuel cell performances (Figure 5) catalyzed by three different Pt/CNT cathode catalysts (Pt/non-oxidized CNT, Pt/oxidized CNT, and Pt/(oxidized + sensitized CNT)) showed that the Pt/(oxidized + sensitized CNT) catalyst prepared by a two-step process

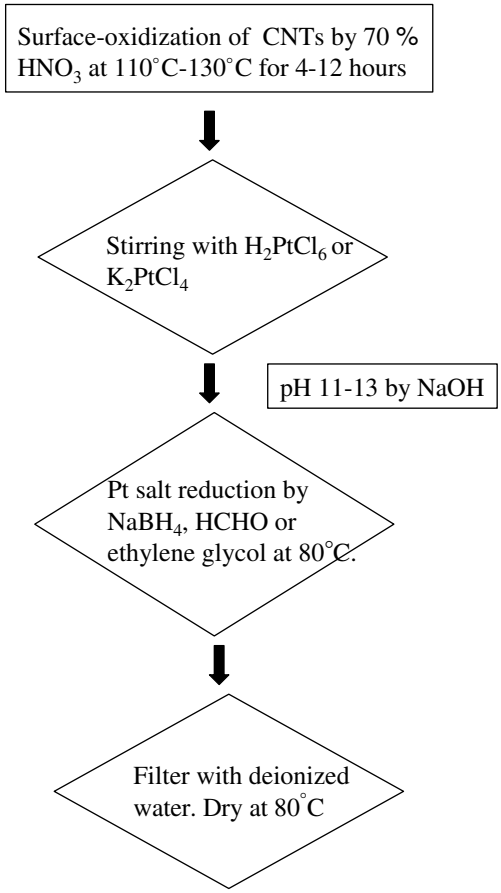

Fig. 3. A typical synthesis process of Pt/CNT catalysts by the electroless deposition method [25, 36, 37].

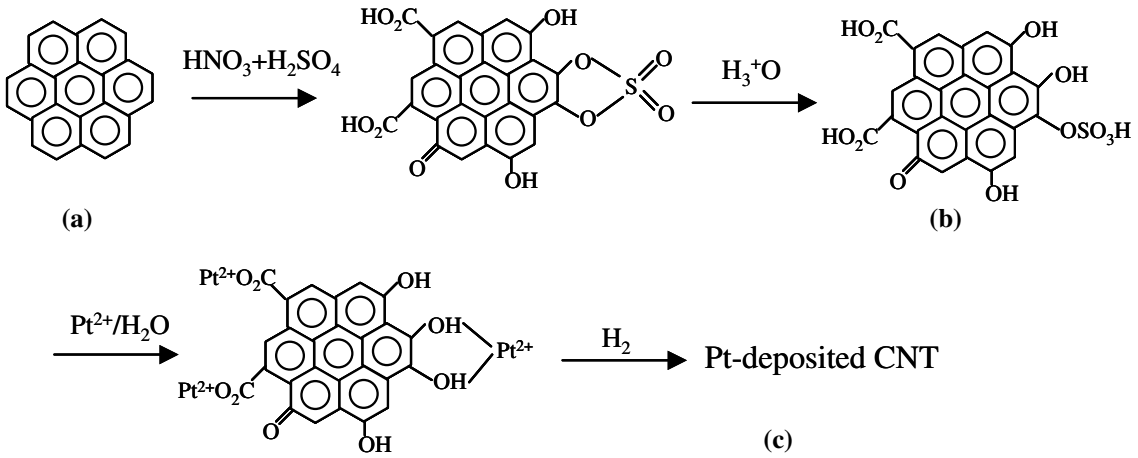

Fig. 4. Scheme of the mechanism of Pt deposition via the oxidation of HNO_3 + H_2SO_4 on the CNT. Reproduced from [40].

gave the best cell performance compared to the other two catalysts [39]. Liu et al. argued that the improved performance of a Pt/CNT catalyst produced by the two-step sensitization activation process might be attributed to the increased wetting of the CNT surface by the $SnCl_2$ sensitization step, resulting in a more uniform Pt deposition.

Li et al. compared two synthesis methods using different reduction agents for Pt deposition on CNTs: one is the reduction of the Pt ion by a HCHO solution (HCHO reduction method), and the other is the reduction of the Pt ion by an ethylene glycol solution (EG method) [25]. The HCHO method was the same as described in Figure 3. In the case of the EG method, the surface-oxidized MWNTs were first suspended in a stirred ethylene glycol solution. The resulting suspension was then added with hexachloroplatinic acid and continuously stirred for 4 h. NaOH was added to adjust the pH of the solution to above 13. After that, the solution was then heated at 140 °C for 3 h to ensure that Pt was completely reduced. The procedure of filtering, washing and drying were the same as the HCHO method. Figure 6 shows the micrograph of Pt/MWNT catalysts by different reduction methods. The HCHO method could give a Pt particle size distribution range from 2 to 9 nm with a mean particle size of 3.4 nm, while the EG method provided a high and homogeneous dispersion of spherical Pt metal nanoparticles, which are in the particle size range from 2 to 5 nm with a mean size of 2.6 nm. This EG method could also give a similar Pt particle size of 2.2 nm on the Pt/Vulcan XC-72 catalyst support. Therefore, the EG method is better than the HCHO method in terms of particle size and distribution uniformity. In addition, they also found that the concentration of ethylene glycol can affect the size of the Pt particles. As shown in Table 2, when pure EG was used as the reducing agent, the Pt particle size was 2 nm. However as the EG solution was diluted by water, the Pt particle size became larger. The electrochemical test at direct methanol fuel cell (DMFC) conditions showed that Pt/MWNT catalysts by EG method could give a cathode activity of 14.7 mA mg^{-1} Pt at 700 mV (vs DHE), which is 2.5 and 6 times larger than those of Pt/MWNT (HCHO method) and Pt/Vulcan (EG method), respectively. This comparison might not be accurate because the mass activity could be largely affected by Pt particle size [44]. However, it is feasible to compare the catalytic mass activity of the Pt/MWNT produced by the EG method with that of Pt/Vulcan, because both of them have almost the same Pt particle sizes. The former showed considerably higher ORR mass activity than the latter. It was interpreted that the higher ORR mass activity of Pt/MWNT produced by the EG method might be attributed to the unique structure and good electrical properties of MWNT, which could improve the water-oxygen mass transport within the catalyst layer and reduce the electric resistance of the catalyst layer if compared to a commercially available Vulcan support. Moreover, an enhanced interaction between Pt and MWNT might be also related to a higher mass activity.

2.1.2. *Sonochemical technique*

The conventional electroless deposition method can produce highly dispersed Pt nanoparticles with small particle sizes. The mean particle size is in the range of

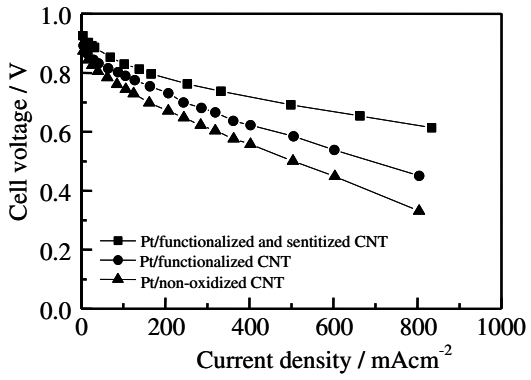

Fig. 5. Polarization curves of different Pt/CNT catalysts from a fuel cell test: O_2, 1 bar; H_2, 1 bar; 50 °C. Reproduced from [39].

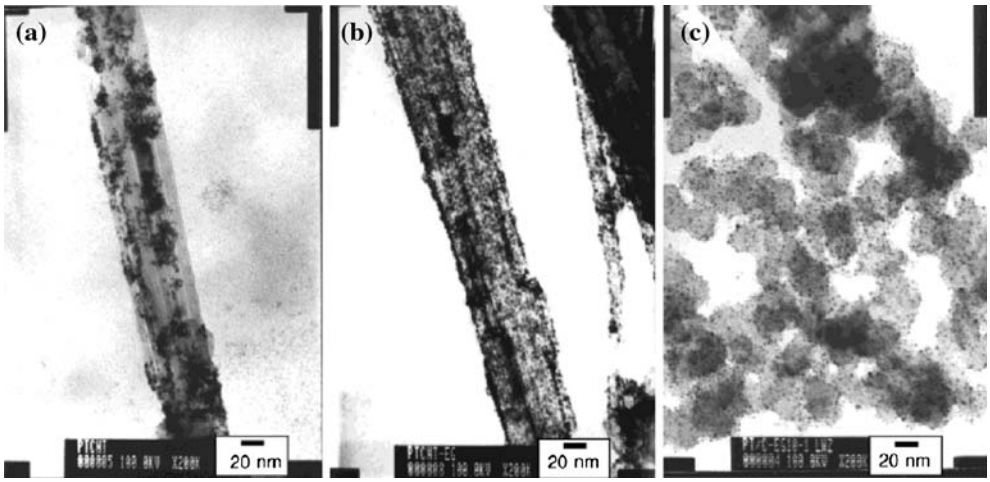

Fig. 6. TEM images of (a) Pt/MWNT (reduction by HCHO), (b) Pt/MWNT (reduction by EG), (c) Pt/Vulcan (reduction by EG) [25].

1–10 nm and the Pt content in Pt/CNT catalyst is below 20 wt%. Recently, Xing introduced a sonochemical technique into the electroless deposition method in order to increase Pt content in the Pt/CNT catalysts [38]. The main purpose of the sonochemical step is to improve the oxidation of the CNT surface by strong nitric and sulphuric acids in order to obtain more surface functional groups. The typical sonochemical treatment of CNTs is as follows: the purified CNTs are added into a mixer-stirred solution of 8.0 M HNO_3 + 8.0 M H_2SO_4 and sonicated in an ultrasonic bath at 60 °C for 2 h to disperse the CNTs. This process could break the big CNT aggregates. After this treatment, CNTs are separated from the acids and washed with deionized water. Finally, the Pt deposition process is almost the same as the conventional electroless deposition method as described in Figure 3.

Figure 7 shows the TEM images of the Pt nanoparticles supported on sonochemically treated CNTs [38]. It can be seen that the Pt nanoparticles are highly dispersed on the surface of CNTs. Such dispersion is much better than those produced by a conventional electroless deposition method. Moreover, it was claimed that the Pt content was increased up to 30 wt% in Pt/CNT catalyst. The obtained Pt particle sizes were ca. 2.7, 3.57, and 4.46 nm for 10, 20, and 30 wt% catalysts, respectively. Although the Pt particle size increased as Pt loading increased, the high dispersion and narrow particle size distribution range were observed at high Pt loading. Since the conventional electroless deposition method cannot break the CNT aggregates effectively, the nitric acids may not easily get into the inside of the CNT aggregates during the HNO_3 refluxing process. In this case, some CNT surfaces inside the aggregates may not be oxidized. In sonochemical process, however, the prolonged and repeated ultrasonic treatments can disperse CNTs more effectively during the refluxing process, and create more uniform surface functional sites on the CNTs. A 48% higher specific active surface area of this Pt/CNT catalyst was observed when compared with a commercially available Pt/Vulcan catalyst at the same Pt loading. For the comparison of electrochemical catalytic activity, the former performed 102% better than the latter one. This sonochemcial technique might be very useful for increasing the CNT surface functional site and the Pt content in Pt/CNT catalysts.

Table 2. Effect of water content in EG solution on the preparation of Pt/MWNT [25]

Water content (%, volume ratio)	Pt particle size (nm)
0	2.0
5	2.5
15	3.2
40	4.0
70	4.5

2.1.3. *Microwave heated polyol process*

Recently, a microwave heated polyol process was employed to synthesize carbon-supported Pt catalysts for fuel cell catalysis [45–50]. The polyol process (ethylene glycol mediated reactions) was mainly used to prepare the colloidal metal particles. In this process, a polyol (ethylene glycol) solution containing catalyst metal precursor salts is refluxed at 393–443 K in order to homogeneously decompose the ethylene glycol and create an active reducing agent for metal ions [45, 49]. A metal support could be optionally present to capture the depositing metal particles in this process. Unlike the conventional conductive heating strategy used to thermally activate the polyol, which has a heterogeneous temperature distribution, the fast heating by microwaves can accelerate the reduction of the metal precursor ions and the nucleation of the metal particle. In addition, the homogeneous microwave heating could reduce the temperature and concentration gradients in the reacting sample solution, resulting in a more uniform environment for the nucleation and growth of metal particles [45, 49]. Therefore, as a rapid, uniform and effective heating method, microwave heating has become an

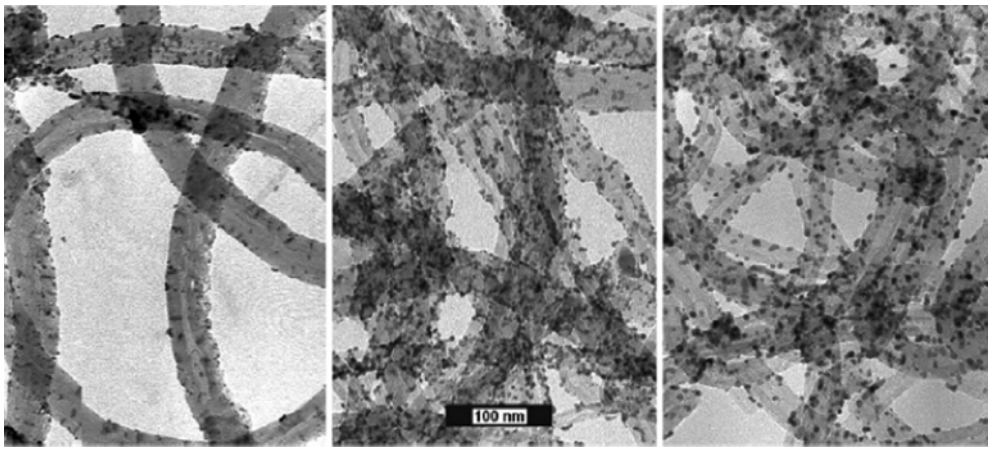

(a) 10 wt % **(b)** 20 wt % **(c)** 30 wt %

Fig. 7. TEM images of Pt nanoparticles deposited on sonochemically treated CNTs [38].

attractive alternative approach for synthesis of carbon-supported Pt catalysts.

Chen et al. prepared Vulcan carbon-supported catalysts with Pt contents of 10, 15, and 20 wt% using a simple microwave procedure [46]. The Pt particle size obtained by this method was 3.5–4 nm with a very narrow particle size distribution. For PtRu/Vulcan catalyst preparation, Yang et al. also successfully deposited the PtRu on the Vulcan support with a particle size of 1.5 nm [47]. The produced PtRu/Vulcan catalysts have a very narrow particle size distribution (± 0.5 nm) and a very high catalyst metal content (PtRu 60 wt%). More recently, several research groups have initiated the synthesis of Pt/CNT or PtRu/CNT catalyst using a microwave heated polylol process [45, 48–50]. The synthesis procedure for Pt/CNT catalysts can be outlined as follows [45]: First, the mixture solution of H_2PtCl_6 + ethylene glycol is prepared with the addition of KOH to adjust the pH. Then, the purified CNTs are added to the mixture while it is being sonicated. After a period of heating in a microwave oven, the resulting suspension is then filtered and washed with acetone and deionized water, and dried at 373 K over night in a vacuum oven. Since ethylene glycol has a high dielectric constant (42.4 at 298 K), the heating process by microwave irradiation could be very fast. During the heating, the temperature of such a suspension of ethylene glycol, Pt salt and CNTs will go up to 170–180 °C. This heating step can decompose ethylene glycol to generate reducing species, i.e. CH_3CHO which then reduces the Pt ion to a Pt metallic particle.

Liu et al. employed a microwave heated polyol process for the synthesis of PEM fuel cell cathode Pt/CNT catalysts [45, 49]. Some highly dispersed Pt nanoparticles on CNTs with Pt particle size of 3.6 ± 0.3 nm were obtained. For the Pt/Vulcan catalyst, on the other hand, the Pt particle size of 3.8 ± 0.3 nm was obtained by the same method. The Pt particle size distribution in the Pt/CNT catalyst was narrower than that of the Pt/Vulcan catalyst. The Pt contents can be high, up to 19.4 wt% in Pt/CNT and 18.9 wt% in Pt/Vulcan, respectively under the same synthesis condition. The slight difference of the Pt content between two different supports might be due to the different surface structure between the CNT and Vulcan. The fuel cell test showed that the Pt/CNT catalyst had greater catalytic activity towards ORR than the Pt/Vulcan catalyst although both catalysts had almost the same Pt particle sizes. In addition, exchange current density for ORR catalyzed by the Pt/CNT catalyst was 2 times larger than that catalyzed by Pt/Vulcan catalyst.

Li et al. also investigated the pH effects on the Pt particle size and uniformity of the Pt/CNT catalyst prepared by the microwave heated polyol process [50]. In their experiments, the pH of ethylene glycol solution containing a H_2PtCl_6 precursor was adjusted by KOH during the deposition of Pt metal on the CNTs. Based on the TEM measurement, the higher pH was found to improve the size, uniformity, and dispersion of Pt nanoparticles on the CNT surfaces. Table 3 shows the Pt particle sizes and distribution ranges of Pt/CNT catalysts prepared at different pH. It can be seen that the Pt particle size can be reduced by increasing the solution pH. TEM images showed that at lower pH range (pH 3.6–5.8), Pt nanoparticles are apparently agglomerated and not well dispersed on CNT surfaces. However, at the pH range of 7.4–9.2, there was less agglomeration and a more uniform dispersion Pt nanoparticle distribution. Therefore, the solution pH plays an important role in controlling the Pt particle size and distribution. The mechanism of the pH effect on the formation of the Pt nanoparticle in ethylene glycol solution was suggested as the following [50, 51]:

$$CH_2OHCH_2OH \rightarrow CH_3CHO + H_2O \tag{2}$$

$$2CH_3CHO + (PtCl_6)^{2-} + 6OH^- \rightarrow 2CH_3COO^- + Pt + 6Cl^- + 4H_2O \tag{3}$$

The resulting acetate in reaction (3) can serve as a stabilizer for Pt colloids through the formation of chelate-type complexes via its carboxyl group. At a low pH, however, a low interaction between acetate and Pt colloids can be expected. Consequently, the poor stabilization of Pt colloids could not protect Pt particles from agglomeration, resulting in larger Pt size and wider particle size distribution. Table 3 also shows that the Pt active surface area determined by the electrochemical method becomes larger with a solution pH increase, which could be attributed to the decrease in the particle size.

2.1.4. *Electrodeposition (potential step deposition method)*

The electrodeposition method used for Pt particle attachment onto the carbon supports has been developed by many research groups to improve the Pt utilization and reduce Pt loading [28, 52–56]. Taylor et al. explored this method and successfully fabricated electrodes with a very low Pt loading [55, 56]. In their method, the Pt was first electrodeposited on the Nafion coated carbon supports in a plating bath. In this way, the Pt ions could diffuse through the surface of the Nafion coating into the carbon support surface to form Pt particles. Smaller Pt particles with diameters of less than 4–5 nm can be deposited on the carbon surface to form a Pt/Carbon catalyst [57]. It was suggested that the ionic path channels inside the Nafion coating could serve as the diffusion path for Pt ions. The Pt particle size of 2–3.5 nm at a Pt loading of less than 0.05 mg cm^{-2} was also obtained. Electrochemical tests showed that a 10-fold increase in mass activity for ORR was achieved in comparison with a conventional electrode catalyzed by an E-TEK catalyst. This result could be attributed to the increase in Pt utilization. However, this approach is strongly limited by the diffusion of Pt ions through a Nafion ionic channel. In order to overcome this limitation, Antoine et al. first impregnated carbon support with H_2PtCl_6, then coated the carbon support with Nafion [54]. In this way, the Pt ions do not need to diffuse across the recast Nafion layer from the external aqueous electrolyte to the carbon support surface, because they are already present on the carbon support surface. A Pt content over 20 wt% in the Pt/C catalyst was achieved with a narrow Pt particle size distribution, i.e., about 2–4 nm. It was expected that this method could increase the Pt content up to 40 wt% with the same Pt particle size distribution.

Table 3. Pt particle size and active specific surface area for Pt/CNT prepared from the synthesis solution with a different pH [50]

Solution pH	Average Pt size (nm)	Pt particle size distribution range (nm)	Active surface area ($m^2\ g^{-1}$)
3.6	5.8	1–10	50.4
5.8	5.2	1–10	56.4
7.4	3.4	1–5.5	80.8
9.2	2.7	1–5	96.4

Several groups have reported the synthesis of Pt/CNT catalysts by this electrodeposition method [58–60]. Wang et al. successfully employed this method to prepare Pt/MWNT catalysts [58]. In their work, the MWNT was directly fabricated on the carbon paper through a chemical vapour deposition process (CVD). An electrodeposited Co catalyst on the carbon paper was employed for MWNT growth. The main function of the Co catalyst was to improve the electrical contact between the MWNTs and the carbon paper. Following the growth of MWNTs on carbon paper, Pt was then electrodeposited on the MWNTs by an electrochemical method in $H_2SO_4 + H_2PtCl_6$ solution. The deposition potential used was 0 V (vs SCE) and the loading of Pt could be controlled by the totally passed charge. Although the deposition process was successful with a Pt loading of 0.2 mg cm^{-2} on the MWNT surface, the average diameter of the Pt particle was too large, i.e. ~25 nm compared to the commercially available Pt/C catalyst. The fuel cell performance catalyzed by a synthesized Pt/MWNT catalyst was also lower than that catalyzed by conventional catalyst at a comparable Pt loading.

Guo et al. employed a three-step process including the electrodeposition method to prepare SWNT-supported Pt catalysts for methanol oxidation [60]. As shown in Figure 8, the first step is to create the surface functional groups. The MWNT paste, which was mixed with mineral oil and packed into a cavity of Teflon tubing was electrochemically activated by potential cycling at a potential scan rate of 200 mV s^{-1} from +1.8 to −0.4 V (vs SCE) in 0.5 M Na_2SO_4 for 10 min. Such an electrochemical activation treatment could produce various oxide functional groups such as carbonyl, carboxylate and hydroxide at the defect sites such as the tube ends and/or the sidewalls of SWNTs. The second step is to form surface octahedral Pt(IV) complexes which are used as the precursors. This step was carried out in a 2.5 mM K_2PtCl_4 + 0.1 M K_2SO_4 aqueous solution by potential cycling from +0.3 to +1.3 V (vs SCE). The lower limit of the potential scan was restricted to +0.3 V in order to prevent the electrodeposition of Pt(IV). The oxygen atom of the functional groups, such as carboxylate, can serve as one of the two axial ligands when the planar complex of Pt(II) is oxidized to form the octahedral complex of Pt(IV). In the final step, the octahedral complexes of Pt(IV) on the SWNT surfaces are electrochemically reduced to Pt metal through potential cycling from +1.6 to −2.5 V (vs SCE) in a 0.1 M H_2SO_4 solution. The Pt/MWNT catalysts obtained by this three-step process have a Pt nanoparticle size of 4–6 nm. The TEM images for this Pt/SWNT catalyst showed the partial aggregation of Pt nanoparticles on the thicker bundles rather than on the thinner bundles or individual tube. Such an aggregation of Pt nanoparticles could be understood based on the assumption that the number of carboxylic acid groups on the thicker bundles was greater than on the thinner bundles.

2.1.5. *Sputter-deposition technique*

A sputtering-deposition method was recently explored to prepare the PEM fuel cell cathode catalysts, aiming at Pt loading reduction and Pt utilization improvement [61, 62]. Mukerjee et al. investigated the oxygen reduction kinetic parameters on a 0.4 mg cm^{-2} Pt loaded electrode on top of which a sputter-deposited Pt film was formed with a load of 0.05 mg cm^{-2} [61]. The Pt sputtered electrode showed an active surface that was 2 times larger and a current density at 0.9 V (vs RHE) that was 4 times larger than that of Pt unsputtered electrode. Hirano et al. prepared a low Pt loading catalyst layer (0.1 mg cm^{-2}) on an uncatalyzed E-TEK electrode using the sputter-deposition technique [62]. The thickness of the sputtered catalyst layer could be decreased to about 1 μm. When compared to a 32 μm E-TEK electrode with a Pt loading of 0.4 mg cm^{-2}, this sputtered electrode showed slightly lower cathode potential and exchange current density at a low current density region than that of the E-TEK electrode. This could be attributed to the lower active surface areas. However, at a high current density region, the sputtered electrode could give a higher ORR potential than that of E-TEK electrode, which could be due to the low mass transport overpotential. Based on their results, the sputter-deposition technique was proposed as a novel electrode synthesis method for a low Pt loading cathode.

More recently, the sputter-deposition technique has been further employed to prepare a CNT-supported Pt catalyst by several research groups. In the efforts of Chen's group [63], the CNTs were first fabricated on the carbon cloth on which the Pt particles were then sputtered. They used a bias-assisted microwave plasma enhanced CVD method to prepare CNTs, which is a slightly different process than that employed by Sun et al. [43] and Wang et al. [58]. An Fe catalyst and a CH_4 + H_2 gas mixture were used for the direct fabrication of CNTs on the carbon cloth at 300 W microwave power and 10 Torr of working pressure. In the process, the length of CNTs could be increased with the increase of negative bias voltage. A bias voltage of −100 V was found to be an optimum condition for Pt sputtering deposition. The employed sputtering current and time were 10 mA and 30 s, respectively. For comparison, the electroless deposition method was also used to deposit Pt particles on the same CNTs. TEM results showed that the sputtering method could generate highly uniformed Pt nanoparticles on CNTs compared to that produced by the electroless deposition method. The Pt particle sizes deposited by the sputtering method were in the range below 2 nm, while those deposited by electroless method produced a particle size range of 2–5 nm on the same CNTs. Sun et al. [64] tried to deposit Pt nanoparticles on nitrogen-containing CNTs (CN_x NTs) for μDMFC application. The CN_x NTs were grown on Si substrate through microwave-plasma-enhanced chemical vapour deposition (MPECVD) using CH_4, N_2 and H_2 gases. For Pt deposition, a DC sputtering technique was employed. Some well-separated Pt nanoparticles were formed with an average diameter of 2 nm on CN_x NTs. Cyclic voltammogram showed that Pt/CN_x NTs catalyst had electrochemical activity towards methanol oxidation.

Their results suggest that the sputter-deposition technique is a better way to deposit small and uniform Pt nanoparticles. This method can also generate a thinner catalyst layer that could give a higher fuel cell cathode performance and, at the same time, reduce the Pt loading considerably. However, with respect to the electrode mass production, the sputter-deposition technique may face some technical challenges.

2.1.6. *γ-Irradiation technique*

It is well known that the colloidal noble metal nanoparticles can be prepared by γ-irradiation-induced reduction of noble metal ions without the addition of a chemical reduction agent. Metal ions can be reduced by some reducing species *in situ* generated in the radiolysis of aqueous solvents. Oh et al. prepared CNT-supported Ag, Pd and Pt–Ru catalysts using this

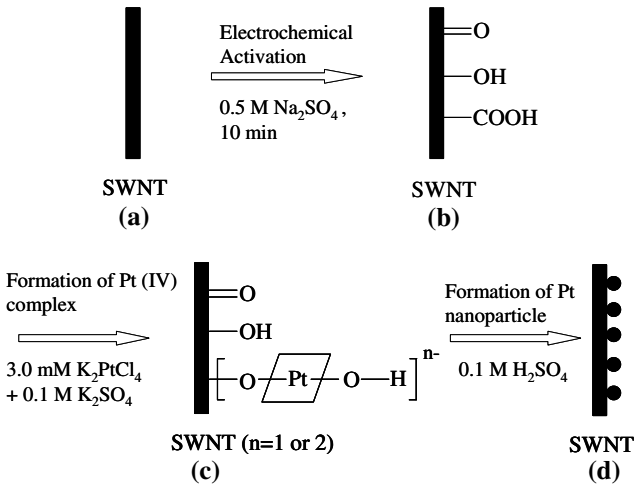

Fig. 8. Schematic diagram of the three-step electrochemical synthesis of Pt nanoparticles on CNTs. Reproduced from [60].

γ-irradiation technique [65]. For example, the procedure to prepare a Pt–Ru/CNT catalyst is as follows: H_2PtCl_6 and $RuCl_3$ were first dissolved in water + 2-propanol solution containing CNTs. The solution was bubbled with nitrogen for 30 min to remove the dissolved oxygen, and was then irradiated by γ-ray from a Co-60 source under atmospheric pressure and ambient temperature. A total irradiation dose of 30 kGy was used for this process. The γ-irradiation can generate the functional groups on the CNT surface, such as hydroxyl and carboxyl groups. The dispersion of noble metal particles on the modified CNT surface might be facilitated by γ-irradiation treatment. Although the noble metal particles could be dispersed on CNTs successfully, the TEM images showed that the Pt-Ru alloy particle size was little bit too large (~15 nm) and their partial aggregation was also observed.

2.1.7. *Self-regulated reduction of surfactants*

Lee et al. reported a novel and simple preparation method, namely the self-regulated reduction of surfactant method, for Pt/CNT and Pt/CNF catalyst synthesis [66]. They deposited the Pt nanoparticles on the sidewalls of sodium dodecyl sulphate (SDS) micelle functionalized onto CNTs or CNFs. SDS was used to modify the surface structures of CNTs or CNFs, and act both as the reducing and protective agents for the deposition of Pt metal. In this way, the external reducing agent is no longer needed [66, 67]. The typical synthesis process for a Pt/CNT catalyst is as follows: CNTs are first capped with SDS micelle and dispersed in a SDS aqueous solution by a sonicator agitating for ~4 h. After this sonication process, the resultant SDS aqueous solution containing dispersed CNTs is immediately refluxed in an oil bath at ~130 °C for ~7 h. During the refluxing process, some of the SDS amphiphiles in the CNT/SDS solution could release 1-dodecanol, which serves as a reducing agent for metal deposition at the refluxing temperature. For the deposition of Pt metal, H_2PtCl_6 was added into the CNT/SDS solution, and was slowly reduced to Pt metal by 1-dodecanol in the micellar core, forming Pt nanoparticles. TEM results confirmed that the Pt particle size deposited on the CNTs and CNFs was very small (1.6–1.87 nm) with a very narrow particle size distribution range of 1–3 nm. It was explanted that the 1-dodecanol, which is released from CNT/SDS solution, reduces the Pt(IV) to Pt(0) and itself will be oxidized into a lipid acid. This lipid acid could alter the SDS-modified CNT framework via the adhesion of carboxylic heads onto the CNT surface. In addition, the co-adsorption of 1-dodecanol and uncapped lipid acid on the Pt particle surface can further undergo esterification, resulting in the link between the Pt nanoparticle and CNT inside a modified SDS template. Consequently the stable Pt/CNT nanocomposite will be produced. The uniform dispersion of Pt particles on the CNTs was found to be strongly dependent on the type of CNT. MWNT or CNF with more defect and roughness surfaces can give more uniform Pt distribution than SWNT. An advantage of this method over conventional surface oxidation treatment method is that it can simply prepare the Pt/CNT or Pt/CNF catalysts without the destruction of carbon nanomaterial surface structures.

2.1.8. *Colloid method*

Yoshitake et al. reported the colloid method for the synthesis of Pt/CNT catalysts in their PEM fuel cell cathode preparation using single-wall carbon nanohorns (SWNH) as the support [68]. The SWHN is a new type of carbon nanotube with a horn-shaped sheath of single-wall graphene sheets. Figure 9(a) shows the structure of a SWNH. The SWNHs were prepared using CO_2 laser ablation. The Pt catalyst was supported on the SWNHs by colloidal method. In the preparation, $NaHSO_3$ and H_2O_2 were added into a H_2PtCl_6 solution to form Pt oxide colloids. Then the SWNH powder was added into the Pt oxide colloid solution where the Pt oxide colloid was adsorbed on the SWNH surface. After eliminating Cl, Na and S ions, the samples were dried and reduced by H_2 gas. The produced Pt/SWNH catalyst showed very homogeneous dispersion of Pt nanoparticles with an average size of 2 nm, as shown in Figure 9(b). The loading of Pt nanoparticle dispersion on the surface of SWNH was less than half of that supported on the conventional carbon black (Vulcan). Based on that, NEC corporation announced a micro fuel cell system with a Pt/SWNH catalyst in 2001 [69]. The PEM fuel cell catalyzed by Pt/SWNH catalysts showed a 20% higher performance than that catalyzed by conventional Pt/C catalysts. The improvement of the fuel cell performance may be attributed to the homogenously dispersed small-sized Pt particle on the SWNH.

2.2. *Pt/carbon nanofiber (Pt/CNF) catalysts*

Recently, the unique properties of carbon nanofibers (CNF) have drawn great interest in a number of applications such as energy storage, catalyst supports, etc. [70]. Carbon nanofibers (carbon filaments or filamentous carbon) were first reported by Hughes and Cambers in 1889 [22]. The CNFs can be grown by catalytic decomposition of certain hydrocarbons over some small metal particles such as iron, cobalt, nickel and their alloys [30, 34]. The diameter of the CNF can be controlled by the size of the catalyst nanoparticles. The usual diameters of CNF are 2–100 nm and lengths are in the range of 5–100 μm. As shown in Figure 10, three types of CNF are well known: fishbone, deck of cards, and parallel. The fishbone (herringbone) type CNF has graphene layers with an angle of 45° to the growth axis. The deck of cards (platelet) type CNF has graphene layers perpendicular to the growth axis. The parallel (tubular) type CNF has graphene layers parallel to the growth axis with multi-wall assembly [34, 71, 72].

Conventional carbon supports, i.e. carbon blacks predominantly have basal graphite planes on their surface. The interaction of such a surface with Pt

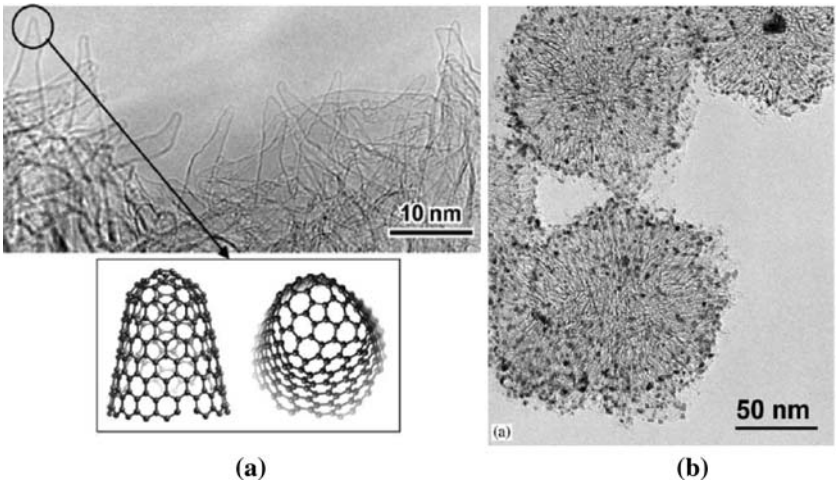

Fig. 9. TEM images of SWNHs nanostructure (a) and Pt/SWNH catalyst (b) [35, 68].

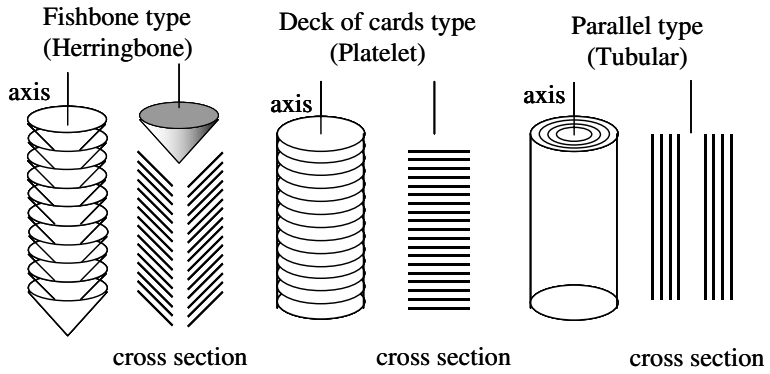

Fig. 10. Schematic representation of three types of CNFs. Reproduced from [34, 71, 72].

particles is very weak. However, the CNF's unique surface structure, namely the regular arrangement of graphite planes with their edges exposed to the outer surface of the fibers, could serve favourable sites for the stabilization of small Pt particles. In addition, the regular arrangement of such sites can provide more uniform distribution of Pt particles on the their surfaces [72].

In the 1970s, Koyama synthesized vapour grown carbon fibers (VGCF) through a process of hydrocarbon gas pyrolysis in the presence of hydrogen at a temperature range of 950–1200 °C [73]. The hydrocarbon gases employed were benzene and methane. CNF, which has excellent mechanical, electrical and thermal properties, should be suitable for catalyst support in PEM fuel cell catalysis.

2.2.1. In situ *colloidal process*

Sasaki et al. explored the vapour grown carbon fibers (VGCFs) for electrode filler and catalyst supports in their PEM fuel cell catalysis study [74, 75]. Figure 11 shows the effect of cathode catalyst VGCF content on cell performance. The cathode with the lowest Pt loading (0.44 mg cm^{-2}) and the high VGCF content (25%) shows the best cell performance. In this way, the Pt loading could reduce 15%, and the corresponding cell performance could be improved especially at the high current density range. The improvement can be attributed to the improved electronic conductivity and Pt utilization if the catalyst is mixed with VGCF which has high electronic conductivity. The improvement at high current density range clearly indicates that the mass transfer process in the catalyst layer can also be improved with the addition of VGCF in the catalyst. The mixtures of VGCF and carbon black (Vulcan XC72) were also explored as the catalyst supports. The Pt/(VGCFs + Vulcan) catalysts prepared via the conventional impregnation technique showed an optimum cell performance at around 10–25% VGCF content.

Three types of CNFs, i.e., platelet, herringbone and tubular were employed as catalyst supports for Pt nanoparticle deposition using an *in situ* colloidal process in which H_2PtCl_6, NaH_2O_3, and H_2O_2 were used as deposition reagents [75, 76]. Table 4 shows the crystallite size of Pt nanoparticles on various carbon supports, synthesized via an *in situ* colloidal impregnation process. X-ray diffraction (XRD) analysis revealed that the morphologies of Pt nanoparticles deposited on different CNFs were strongly dependent on the type of CNF. In the case of the tubular type, Pt particles were deposited

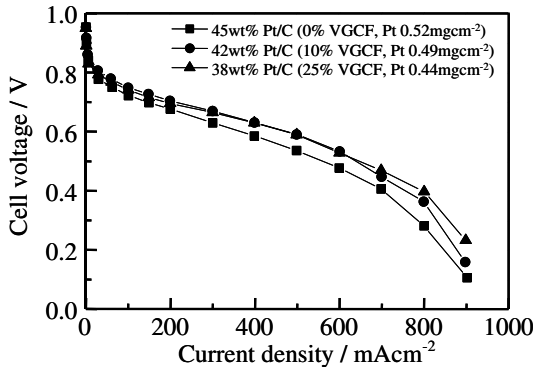

Fig. 11. I–V characteristics of fuel cell with cathode containing different amounts of VGCFs. Reproduced from [74].

locally and agglomerated at the edges of CNFs. For the herringbone type, although the dispersion of Pt particles was better than that of tubular type, local aggregation of Pt particles could be observed. The platelet type gives the best results in terms of small Pt nanoparticle size, uniform dispersion, and less local agglomeration. The favourable order of Pt dispersion was platelet > herringbone > tubular. On the other hand, kinetic current density per real surface area, J_k, for ORR obtained from the rotating disk electrode (RDE) method gave the following order: herringbone > platelet > tubular.

2.2.2. *Physical surface pre-treatment technique*

Ota's group developed a novel physical surface pre-treatment method in order to increase the anchoring sites of a synthesized VGCF surface [77]. The VGCFs were physically ground using a high-speed grinder for 0, 5, 10, and 20 min before depositing the Pt metal. This treatment could physically increase the surface defects of VGCFs. Figure 12 shows the TEM photographs of Pt/VGCF catalysts with and without the physical surface treatment. On the physically pre-treated VGCFs, smaller and more homogeneous Pt nanoparticles compared to that of untreated VGCF were generated because the grinding process can produce many more surface defects which then serve as anchoring sites for Pt nanoparticles. The longer the grinding time, and the smaller the Pt particle size, the better is the resulting dispersion. The electrochemical measurements showed that ORR catalytic activities such as specific and mass activities of Pt/VGCF catalysts were strongly dependent on the length of time of the physical pre-treatment. For example, the specific activity was decreased with the increase of grinding time, which is understandable based on the effect on the size of Pt particles [44]. In the case of mass activity, maximum activity was observed at 5–10 min grinding time.

The physical surface pre-treatment technique for high Pt dispersion might be a more useful method to generate Pt anchoring sites on the inert surface of VGCFs compared to the chemical nitric acid treatments.

Table 4. Crystallite size of Pt nanoparticles on various CNFs [75]

Carbon supports	Pt particle size (nm)
Vulcan XC-72R	3.4
CNF-platelet	3.3
CNF-herring	3.9
CNF-tubular	3.6
VGCF	5.6

2.2.3. In situ *polymerization of acryclonitrile*

Zhang et al. introduced a synthesis method for Pt/CNF catalyst preparation [78] called *in situ* polymerization of acryclonitrile, in which the acryclonitrile is polymerized in a porous anodic aluminium oxide (AAO) membrane template. Figure 13 shows the synthesis procedure. For steps (a) to (b), the hexagonally packed porous AAO membrane is first fabricated by a two-step anodization using 0.3 M oxalic acid aqueous solution at 40 V and 50 °C. This step process forms pores in AAO membrane. Then, the pores are widened by a chemical etching in 5% phosphorous acid at 30 °C. From steps (b) to (c), the AAO templates are immersed in a distilled acrylonitrile monomer (CH_3CH_2CN) containing 0.1 wt% 2,2′-azo-bis-isobutyronitrile (AIBN) and 1 wt% Pt(II) acetylacetonate [$Pt(acac)_2$]. Steps (c) to (d) is the polymerization process. The polymerization and cyclization are carried out at 50 and 220 °C, respectively in the AAO templates for 10 h. Steps (d) to (e) remove the residual Al substrate in a solution containing 0.1 M $CuCl_2$ and HCl. The polyacrylonitrile (PAN) nanofibers in AAO membrane were further pyrolyzed at 700 °C under high vacuum for 6 h in steps (e)–(f). Finally, from steps (f)–(g), the AAO template was removed by dissolution in a 6 M NaOH aqueous solution. The formed Pt/CNF catalyst was then dried in liquid CO_2 to reduce the aggregation of nanofibers. X-ray photoelectron spectroscopy (XPS) analysis confirmed that more than 90% of the Pt(II) acetylacetonate was reduced to Pt metal during pyrolysis of the PAN nanofibers.

In this way, the deposited Pt nanoparticles had an average size of 2.2 nm with a distribution range of 1–4 nm. The synthesized Pt/CNF catalyst showed a 0.94 V (vs Ag/AgCl) onset potential for ORR, and higher catalytic activity compared to that of Pt/C catalyst synthesized by a bulk polymer pyrolysis method without an AAO template.

Finally, CNT and/or CNF-supported Pt electrocatalyst synthesis methods mentioned above are summarized in Table 5.

3. Conclusions

CNT and/or CNF, which have unique structures and excellent mechanical, thermal and electric properties have been explored as novel catalyst supports in efforts to reduce the catalyst layer Pt loading through increasing Pt utilization. Since the 1990s, there have been many pioneering works that focused on the synthesis of Pt/CNT and/or Pt/CNF catalysts for PEM fuel cell catalysis.

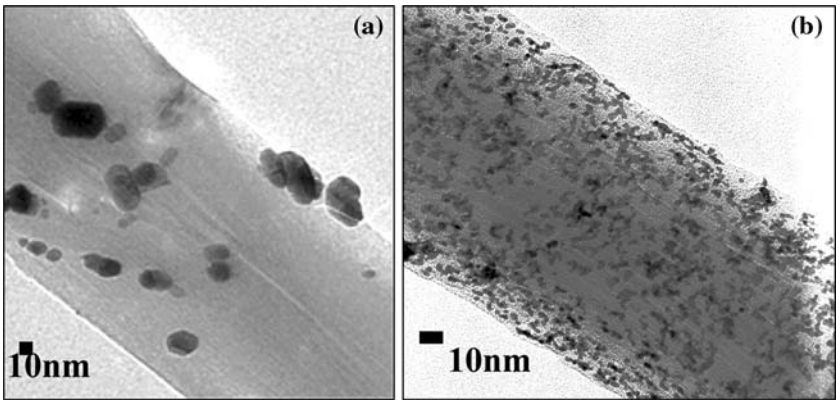

Fig. 12. TEM images of Pt nanoparticles on VGCFs treated on 0 min (a) and 10 min (b) [77].

These works have revealed that the morphology and catalytic activity of Pt/CNT and Pt/CNF catalysts are strongly affected by their synthesis methods.

For the synthesis of CNT-supported Pt catalysts, several catalyst synthesis methods such as electroless deposition, sonochemcial technique, microwave heated polyol process, electrodeposition, sputter-deposition technique, γ-irradiation technique, self-regulated reduction technique of surfactants, and the colloid method are reviewed in this paper. In particular, due to the inert property of the CNT surface, the surface oxidation treatment in HNO_3 or HNO_3 + H_2SO_4 to obtain the surface functional groups such as hydroxyl, carboxyl and carbonyl is necessary for effective deposition of Pt nanoparticles on the CNT surfaces. The created functional groups, which have a strong effect on the formation of the favourable morphology of catalysts, can serve as the anchoring sites for Pt ions. Rajalakshmi et al. [37] confirmed that the Pt/CNT with a smaller Pt particle size and more uniform particle distribution has higher ORR activity compared to that catalyzed by a non-oxidized CNT-supported Pt catalyst. Liu et al. [39] concluded that the functionalization of CNTs by a two-step sensitization-activation treatment was more effective than a conventional surface oxidation treatment for Pt dispersion and ORR activity. The sonochemical technique can also provide an effective way of allowing for CNT surface functional site increases during the oxidation treatment in acidic solution [38]. This technique could increase the Pt content up to 30 wt% in the Pt/CNT catalyst through increasing the surface functional groups. A γ-irradiation technique was also employed to create surface functional groups on CNTs without surface oxidation treatment and the addition of a chemical reduction agent [65]. The average Pt particle size of 1.6–1.87 nm with a narrow particle size distribution of 1–3 nm was obtained by this technique. The preparation of Pt/CNT catalysts via self-regulated reduction of surfactants could be another useful method to deposit Pt particles on the CNTs without acid treatment-induced destruction of CNT surfaces [66]. Finally the sputter-deposition technique can provide low Pt loading and thinner catalyst layer [63].

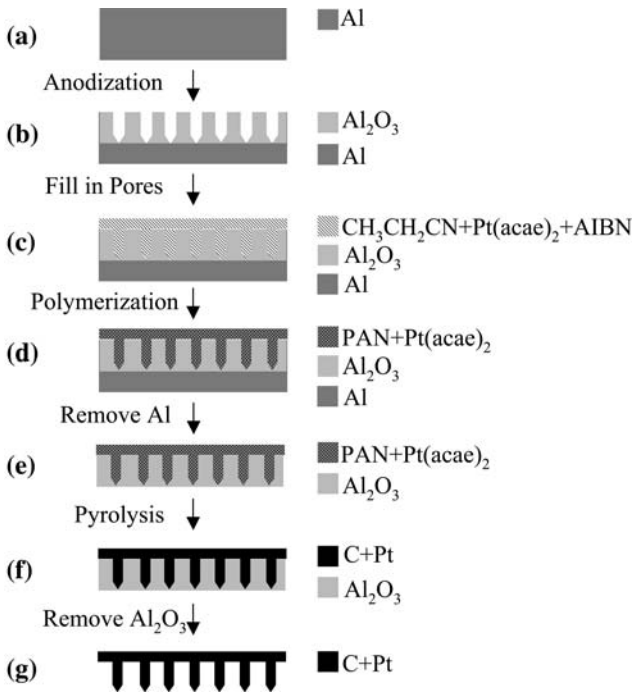

Fig. 13. A schematic diagram of the fabrication of Pt/CNF catalyst using *in situ* polymerization of acrylonitrile. Reproduced from [78].

Compared to the research of Pt/CNT catalysts, Pt/CNF catalysts seem to be less attractive, although several promising results have been reported in PEM fuel cell cathode catalysis. Sasaki et al. [75] found that the platelet type CNFs could provide smaller and more homogeneous Pt particles compared to other types of CNFs such as the herringbone and tubular. When CNF was used as the electrode filler, a 25% CNF filler contained cathode catalyst layer showed better fuel cell performance. This method can also be used to reduce Pt loading [74]. The physical surface treatment to VGCFs using a grinder by Ota's group can increase the Pt ion anchoring sites on VGCFs surface [77]. In this way, the highly dispersed Pt nanoparticles were obtained and the ORR catalytic activity improved considerably.

Table 5. Summarization of synthesis methods for CNT and/or CNF-supported Pt electrocatalysts

Synthesis method	Catalyst	Mean metal particle size (nm)	Particle size range (nm)	Pt content (wt%)	Catalyst performance	Reference
Electroless deposition (two step sensitization)	Pt/MWNT	–	3–5	19.6	676 mV at 500 mA cm^{-2} (PEFC test)	[37]
	Pt/MWNT	2.6	2–5	10	400 mV at 186 mA cm^{-2} (DMFC test)	[25]
	Pt/MWNT	–	1–5	–	690 mV at 500 mA cm^{-2} (PEFC test)	[39]
		4.5	1–9	30		
Sonochemical technique	Pt/MWNT	3.6	–	20	–	[38]
		2.7	–	10		
Microwave technique	Pt/CNT	3.8	2–6	19.4	750 mV at 500 mA cm^{-2} (PEFC test)	[45]
Electrode position	Pt/SWNT	5.3	4–6	–	–	[60]
Sputtering technique	Pt/MWNT	~2	–	–	–	[63]
γ-irradiation technique	Pt–Ru/SWNT	15	–	–	–	[65]
Self-regulated reduction of surfactant	Pt/SWNT	1.8	1–3			
	Pt/MWNT		–	–	–	[66]
	Pt/CNF	1.6	1–3			
Colloid	Pt/SWNH	2	–	–	500 mV at 200 mA cm^{-2} (PEFC test)	[68]
		3.3 (platelet)			600 mV at 500 mA cm^{-2} (PEFC test)	
In situ colloid	Pt/CNF	3.9 (herringbone)		20		[75]
		3.6 (tubular)				
	Pt/VGCF	5.6				
Physical surface treatment	Pt/VGCF	–	–	20	600 mA/mg_{pt} at 900 mV (RHE) PEFC test (half cell test)	[77]
In situ polymerization of acryclonitrile	Pt/CNF	2.2	1.5–2.5	–	ca. 0.65 mA cm^{-2} at 700 mV (Ag/AgCl) (half cell test)	[78]

As a practical application of a carbon nanotube-supported catalyst in a fuel cell system, NEC corporation announced a microfuel cell catalyzed by a carbon nanohorn-supported Pt catalyst (Pt/CNH) in 2001 [69]. It was claimed that the micro fuel cell system, catalyzed by Pt/CNH, could improve 20% of cell performance compared to that catalyzed by a conventional Pt/C catalyst. Such a practical application of CNT suggests that CNT and/or CNF have great potential to reduce catalyst layer Pt loading through their unique ways of Pt utilization improvement.

Acknowledgements

We wish to thank the Institute for Fuel Cell Innovation, National Research Council Canada (NRC_IFCI) for its financial support. Discussions with Dr. Zhong-Sheng Liu and Dr. Dave Ghosh are deeply appreciated.

References

1. J. Larminie and A. Dicks, *Fuel Cell Systems Explained* (John Wiley & Sons, New York, 2000), pp. 61–108.
2. M. Arita, *Fuel Cells* **2** (2002) 10.
3. DOE FY 2002&2004 Annual Progress Reports.
4. L. Zhang, J. Zhang, D. Wilkinson and H. Wang, *J. Power Sources*, DOI: 10.1016/j.jpowsour.2005.05.069.
5. N. Sato, *Oyo Buturi* **72** (2003) 857.
6. H.A. Gasteiger, S.S. Kocha, B. Sompalli and F.T. Wagner, *Appl. Catal. B: Environ.* **56** (2005) 9.
7. N.P. Brandon, S. Skinner and B.C.H. Steele, *Annu. Rev. Mater. Res.* **33** (2003) 183.
8. DOE FY 2000 Annual Progress Report.
9. C. Jaffray and G. Hards, *in* W. Vielstich and H.A. Gasteiger, *Handbook of Fuel Cells – Fundamentals, Technology and Applications*, Vol. 3, Chapter 41 (John Wiley & Sons, New York, 2003), pp. 509–513.
10. K. Kinoshita, *Electrochemical Oxygen Technology* (John Wiley & Sons, New York, 1992), pp. 19.
11. K. Kordesch and G. Simader, *Fuel Cells and their Applications* (VCH, New York, 1996), pp. 3–93.
12. D.M. Bernardi and M.W. Verbrugge, *J. Electrochem. Soc.* **139** (1992) 2477.
13. T. Toda, H. Igarashi, H. Uchiada and M. Watanabe, *J. Electrochem. Soc.* **146** (1999) 3750.
14. T.R. Ralph and M.P. Hogarth, *Platinum Metals Rev.* **46** (2002) 3.
15. D. Thompsett, *in* W. Vielstich and H.A. Gasteiger (eds), *Handbook of Fuel Cells – Fundamentals, Technology and Applications*, Vol. 3, Chapter 37 (John Wiley & Sons, New York, 2003), pp. 467–480.
16. O. Savadogo and P. Beck, *J. Electrochem. Soc.* **143** (1996) 3842.
17. J. Shim, C.R. Lee, H.K. Lee, J.S. Lee and E.J. Cairns, *J. Power Sources* **102** (2001) 172.
18. K. Ota, A. Ishihara, S. Mitsushima, K. Lee, Y. Suzuki, N. Horibe, T. Nakagawa and N. Kamiya, *J. New. Mat. Electrochem. Systems* **8** (2005) 25.
19. S. Mukerjee and S. Srinivasan, *J. Electroanal. Chem.* **357** (1993) 201.
20. G. Tamizhman and G.A. Capuano, *J. Electrochem. Soc.* **141** (1994) 968.
21. T. Tada, *in* W. Vielstich and H.A. Gasteiger (eds), *Handbook of Fuel Cells – Fundamentals, Technology and Applications*, Vol. 3, Chapter 38 (John Wiley & Sons, New York, 2003), pp. 481–488.
22. T.V. Hughes and C.R. Chambers, US Patent 405,480 (1889).
23. S. Iijima, *Nature* **354** (1991) 56.
24. H. Dai, *Surface Sci.* **500** (2002) 218.
25. W. Li, C. Liang, W. Zhou, J. Qiu, Z. Zhou, G. Sun and Q. Xin, *J. Phys. Chem. B* **107** (2003) 6292.
26. A. Thess, R. Lee, P. Nikolaev, H. Dai, P. Petit, J. Robet, C. Xu, Y.H. Lee, S.G. Kim, A. Rinzler, D.T. Colbert, G. Scuseria, D. Tomanek, J.E. Fischer and R. Smalley, *Science* **273** (1996) 483.
27. P. Serp, M. Corrias and P. Kalck, *Appl. Catal. A: Gen.* **253** (2003) 337.

28. S.D. Thompson, L.R. Jordan and M. Forsyth, *Electrochim. Acta* **46** (2001) 1657.
29. T. Matsumoto, T. Komatsu, H. Nakano, K. Arai, Y. Nagashima, E. Yoo, T. Yamazaki, M. Kijima, H. Shimizu, Y. Takasawa and J. Nakamura, *Catal. Today* **90** (2004) 277.
30. N.M. Rodriguez, *J. Mater. Res.* **8** (1993) 3233.
31. R.P. Raffaelle, B.J. Landi, J.D. Harris, S.G. Bailey and A.F. Hepp, *Mater. Sci. Eng. B* **116** (2005) 233.
32. M. Endo, Y.A. Kim, T. Hayasi, K. Nishimura, T. Matusita, K. Miyashita and M.S. Dresselhaus, *Carbon* **39** (2001) 1287.
33. M. Inagaki, K. Kaneko and T. Nishizawa, *Carbon* **42** (2004) 1401.
34. K.P.D. Jong and J.W. Geus, *Catal. Rev.-Sci. Eng.* **42** (2000) 481.
35. S. Iijima, *Physica B* **323** (2002) 1.
36. W. Li, C. Liang, W. Zhou, J. Qiu, H. Li, G. Sun and Q. Xin, *Carbon* **42** (2004) 423.
37. N. Rajalakshmi, H. Ryu, M.M. Shaijumon and S. Ramaprabhu, *J. Power Sources* **140** (2005) 250.
38. Y. Xing, *J. Phys. Chem. B* **108** (2004) 19255.
39. Z. Liu, X. Lin, J.Y. Lee, W. Zhang, M. Han and L.M. Gan, *Langmuir* **18** (2002) 4054.
40. R. Yu, L. Chen, Q. Liu, K.L. Tan, S.C. Ng, H.S.O. Chan, G.Q. Xiu and T.S.A. Hor, *Chem. Mater.* **10** (1998) 718.
41. H. Hirua, T.W. Ebbesen and K. Tanigaki, *Adv. Mater.* **7** (1995) 275.
42. T.W. Ebbesen, H. Hirua, M.E. Bisher, M.M.J. Treacy, J.L. Shreeve-Keyer and R.C. Haushalter, *Adv. Mater.* **8** (1996) 155.
43. X. Sun, R. Li, D. Villers, J.P. Dodelet and S. Desilets, *Chem. Phys. Lett.* **379** (2003) 99.
44. K. Kinoshita, *J. Electrochem. Soc.* **137** (1990) 845.
45. Z. Liu, L.M. Gan, L. Hong, W. Chen and J.Y. Lee, *J. Power Sources* **139** (2005) 73.
46. W.X. Chen, J.Y. Lee and Z. Liu, *Chem. Commun.* (2002) 2588.
47. B. Yang, Q. Lu, Y. Wang, L. Zhuang, J. Lu and P. Liu, *Chem. Mater.* **15** (2003) 3552.
48. Z. Liu, J.Y. Lee, W. Chen, M. Han and L.M. Gan, *Langmuir* **20** (2004) 181.
49. W. Chen, J. Zhao, J.Y. Lee and Z. Liu, *Mater. Chem. Phys.* **91** (2005) 124.
50. X. Li, W.X. Chen, J. Zhao, W. Xing and Z. D. Xu, Carbon, in press.
51. J. Yang, T.C. Deivaraj, H.P. Too and J.Y. Lee, *Langmuir* **20** (2004) 4241.
52. S.D. Thompson, L.R. Jordan, A.K. Shukla and M. Forsyth, *J. Electroanal. Chem.* **515** (2001) 61.
53. H. Kim, N.P. Subramanian and B.N. Popov, *J. Power Sources* **138** (2004) 14.
54. O. Antoine and R. Durand, *J. Electrochem. Solid-State Lett.* **4** (2001) A55.
55. E.J. Taylor, E.B. Anderson and N.R.K. Vilambi, *J. Electrochem. Soc.* **139** (1992) L45.
56. N.R.K. Vilambi, E.B. Andersion and E. J. Taylor, US Patent 5,084,144 (1992).
57. K. Lee, A. Ishihara, S. Mitsushima, N. Kamiya and K.-I. Ota, *J. Electrochem. Soc.* **151** (2004) A639.
58. C. Wang, M. Waje, X. Wang, J.M. Tang, R.C. Haddon and Y. Yan, *Nano Lett.* **4** (2004) 345.
59. Z. He, J. Chen, D. Liu, H. Zhou and Y. Kuang, *Diamond Relat. Mater.* **13** (2004) 1764.
60. D.J. Guo and H.L. Li, *J. Electroanal. Chem.* **573** (2004) 197.
61. S. Mukerjee, S. Srinivasan and A.H. Appleby, *Electrochim. Acta* **38** (1993) 1661.
62. S. Hirano, J. Kim and S. Srinivasan, *Electrochim. Acta* **42** (1997) 1587.
63. C.C. Chen, C.F. Chen, C.H. Hsu and I.H. Li, *Diamond Relat. Mater.* **14** (2005) 770.
64. C.L. Sun, L.C. Chen, M.C. Su, L.S. Hong, O. Chyan, C.Y. Hsu, K.H. Chen, T.F. Chang and L. Chang, *Chem. Mater.* **17** (2005) 3749.
65. S.D. Oh, B.K. So, S.H. Choi, A. Gopalan, K.P. Lee, K.R. Yoon and I.S. Choi, *Mater. Lett.* 59 (2005) 1121.
66. C.L. Lee, Y.C. Ju, P.T. Chou, Y.C. Huang, L.C. Kuo and J.C. Oung, *Electrochem. Commun.* **7** (2005) 453.
67. C.L. Lee, C.C. Wan and Y.Y. Wang, *Adv. Funct. Mater.* **11** (2001) 344.
68. T. Yoshitake, Y. Shimakawa, S. Kuroshima, H. Kimura, T. Ichihashi, Y. Kudo, D. Kasuya, K. Takahashi, F. Kokai, M. Yudasaka and S. Iijima, *Physica B* **323** (2002) 124.
69. http://www.nec.co.jp/press/ja/0108/3002.html.
70. C.A. Bessel, K. Laubernds, N.M. Rodriguez and R.T.K. Baker, *J. Phys. Chem. B* **105** (2001) 1115.
71. Y.A. Zhu, Zh.J. Sui, T.J. Zhao, Y.Ch. Dai, Zh.M. Cheng and W.K. Yuan, *Carbon* **43** (2005) 1694.
72. Z.R. Ismagilov, M.A. Kerzhentsev, N.V. Shikina, A.S. Lisitsyn, L.B. Okhlopkova, Ch.N. Barnakov, M. Sakashita, T. Iijima and K. Tadokoro, *Catal. Today* **102**(103) (2005) 58.
73. T. Koyama, *Carbon* **10** (1972) 757.
74. K. Sasaki, K. Shinya, S. Tanaka, A. Furukawa, K. Ando, T. Kuroki, H. Kusaba and Y. Teraoka, Nanostructuring of PEFC electrode catalysts using carbon nanofibers, Abstract of the 206th Electrochemical Society meeting, Honolulu, 3–8 October (2004) Abstract # 1912.
75. K. Sasaki, K. Shinya, S. Tanaka, A. Furukawa, K. Ando, T. Kuroki, H. Kusaba and Y. Teraoka, Nanostructuring of cathode catalysts for polymer electrolyte fuel cells, Proceeding of the 11th FCDIC Fuel Cell Symposium, Tokyo, Japan, 18–19 May (2003) pp. 239–242.
76. K. Shinya, K. Sasaki, H. Kusaba and Y. Teraoka, PEFC electrode catalysts supported on carbon nanofibers: nanostructure and catalytic properties, Proceeding of the 45th Battery Symposium in Japan, Kyoto, Japan, 27–29 November (2004), pp. 46–46.
77. A. Asami, S. Iinou, A. Ishihara, S. Mitsushima, N. Kamiya and K.I. Ota, Application of Pt/VGCF as cathode for PEFC, Proceeding of the 24th Annual Meeting of Hydrogen Energy Systems Society of Japan, Saitama, Japan, 10–11 December (2004) pp. 16–19.
78. L. Zhang, B. Cheng and E.T. Samulski, *Chem. Phys. Lett.* **398** (2004) 505.